Failure Analysis for Coming out of Shaft from Shrink-Fitted Ceramics Sleeve

Nao-Aki NODA[1], Dedi SURYADI[2], Seiichi KUMASAKI[3]
Yoshikazu SANO[4], Yasushi TAKASE[5]

[1,2,3,4,5]Department of Mechanical Engineering, Kyushu Institute of Technology,

1-1 Sensui-cho Tobata-ku, Kitakyushu-shi 804-8550, Japan

[1]Email: noda@mech.kyutech.ac.jp

Abstract

This paper deals with failure analysis for coming out of the steel shaft from ceramics sleeve connected by shrink fitting. Only low shrink fitting ratio can be applied because of the brittleness of the ceramics sleeve. However, the steel shafts may be loosening out from the ceramics sleeve under such low shrink fitting ratio. In this study, the coming out behavior of the shaft during rotation is analyzed by the finite element method. The roller rotation is replaced by shifted load in the circumferential direction on the fixed roller. It is found that the load rotation can be approximated by the discrete load shifting at the interval angle $\theta_0=12^o$ within 1% error. The effect of the shrink fitting ratio on the coming out of the shaft is discussed as well as several other parameters, such as Young's modulus of the shaft, the friction coefficient, magnitude of the load, and geometry of the shaft. Furthermore, it is found that the shear stress distribution at the shrink-fitted area may be useful for evaluating whether the coming out occurs or not.

Keywords: *Coming out of shaft, Ceramics sleeve, Shrink Fitting, Finite Element Method, Roller structure*

Nomenclature

δ	Diameter different [mm]	a	Outer diameter of the sleeve [mm]
d	Inner diameter of the sleeve [mm]	b	Inner diameter of the sleeve [mm]
T	Sleeve thickness [mm]	N	Number of cycle
t	Shaft thickness [mm]	E_{sl}	Young's modulus of the ceramics sleeve [GPa]
L	Contact length [mm]	E_{sh}	Young's modulus of the steel shaft [GPa]
w	Distributed load on the roller surface [N/mm]	θ_0	Interval of load shift angle in the simulation
ρ	Mass Density [kg/m^3]	u_{zA}	Displacement at point A [mm]
ν	Poisson's ratio	u_{zC}	Displacement at center point [mm]
μ	Friction coefficient	σ_r	Radial stress on the contact part [MPa]
δ/d	Shrink fitting ratio	τ_{rz}	Shear stress at z-direction [MPa]

1 Introduction

Steel conveying rollers are used in the heating furnace as shown in Figure 1 to produce high-quality steel plates for automobiles. Figure 2(a) shows the conventional roller whose inside is cooled by water circulation to reduce the temperature although causing some energy loss and maintenance cost. The steel sleeve and steel shafts are usually connected by shrink fitting and bonded by welding, and the steel sleeve is coated by ceramics on the surface to improve wear resistance. However, the thermal expansion mismatch may induce surface failures such as crack, peeling, wearing resulting in short roller life [1].

Figure 2(b) shows a new ceramics roller consisting of steel shafts at both ends and ceramics sleeve having high heat resistance, wear resistance [2], and corrosion resistance [3]. All ceramics sleeve may prevent most of the defects observed at coated ceramics, and therefore, the roller life can be extended significantly. Since adhesive bonding and metal bonding have very low strength under high temperature, only shrink fitting can be applied for ceramics sleeve and steel shaft connection used in the heating furnace [4-7]. The thermal expansion coefficient of steel is about four times larger than that of ceramics having low fracture toughness [8, 9], attention should be paid to the risk of ceramics sleeve fracture.

In the previous study the authors have considered similar ceramics structures under high temperature environment in continuous galvanizing line [10, 11], in the continuous pickling line [12], and in the heating furnace [13]. It should be noted that only low shrink fitting ratio can be applied for those structures because of the ceramics brittleness.

As an example, similar all ceramics rolls have been successfully developed to be used in a molten metal bath in continuous galvanized steel line [9-11]; however, coming out of the shaft was observed several times in prototype rolls. Since sliding bearings for rolls and rollers do not restrict the axial movement of the shaft, the coming out can be problematic. Even when the shaft movement is restricted within a small allowable range, the coming out of the shaft may cause local thrust loading, frictional heat generation, and wear preventing smooth rotation of the roller. Previously, Truman and Booker investigated micro-slipping between the gear hub and shaft connected by shrink fitting [14]. Antony analyzed contact separation for rotating thermos-elastoplastic shrink fit assembly [15]. However, few failure studies are available for coming out of the shaft from the shrink-fitted ceramics sleeve.

In this paper, therefore, the coming out behavior of the steel shaft from the ceramics sleeve will be considered during operation. The finite element method is applied to simulate the behavior. Then, several mechanical factors will be considered to understand the coming out of the shaft.

2 Analysis conditions

2.1 Shrink fitting connection with roller dimensions

Figure 3 shows dimensions of the roller considered whose outer diameter D=300mm. Here, the roller consists of ceramics sleeve and steel shaft connected by shrink fitting. The shrink fitting ratio is defined as δ/d, where δ is the diameter difference and d is the inner diameter of the sleeve d=240 mm. The shrink fitting connection was analyzed in the previous studies [4-7, 12, 13, 16]. In ref. [4], the ceramics roller structure was studied without considering thermal stress when a ceramics sleeve and steel solid shafts are connected by shrink fitting at both ends. The results show that for larger shrink fitting ratio $\delta/d \geq 0.2\text{x}10^{-3}$, the stress due to distributed load $\sigma_{\theta b}$ becomes constant independently from δ/d. The constant value coincides with the results when the sleeve and shafts are perfectly bonded. In other words, if $\delta/d \geq 0.2\text{x}10^{-3}$, the sleeve and shafts can be treated as a unit body. Moreover, in ref. [13], the ceramics roller structure used in the heating furnace was studied focusing on thermal stress at the shrink fitting portion. The result shows that the maximum thermal stress can be reduced by using the small thickness of the steel shaft [13].

Table 1 shows mechanical properties of the materials. The shaft material is assumed as alloy steel, which is relatively inexpensive but tough enough, and the sleeve material is silicon nitride. Thermal expansion coefficients are also indicated in Table 1.

2.2 Inertial force effect due to roller rotation

In the first place, inertial force effect during the roller rotation will be considered by assuming two-dimensional rotating disk model with a circular hole as shown in Figure 4. Here, the maximum rotating angular velocity ω=33 rad/s can be estimated from the data for the roughing mill [17]. Although the roller data for heating furnace are not available in [17], the carrying speed is nearly the same as the one of roughing mill. When the ceramics sleeve is rotating with the angular velocity ω, the stresses $\sigma_\theta(r)$, $\sigma_r(r)$ appearing at r=r are expressed the equation (1) [18].

$$\sigma_\theta(r) = \frac{3+\nu}{8}\rho\omega^2\left[b^2 + a^2 + \frac{a^2b^2}{r^2} - \frac{1+3\nu}{3+\nu}r^2\right],$$
$$\sigma_r(r) = \frac{3+\nu}{8}\rho\omega^2\left[b^2 + a^2 - \frac{a^2b^2}{r^2} - r^2\right] \quad (1)$$

where a is outer radius, b is inner radius, r is radius at the point, ν is Poisson's ratio, ρ is mass density. By substituting b=120mm, a=150mm, r=b=120mm, ν=0.28, ρ=3200 kg/mm^3 in Fig. 3 into (1), we have $\sigma_\theta(b)$=0.073MPa, $\sigma_r(b)$=0 and the radius expansion $\Delta b=\varepsilon_\theta \cdot b=\sigma_\theta(b)/E_{sh}$=2.94x10^{-5} mm.

Here we only consider the ceramics sleeve rotation without considering the shaft rotation to estimate the dynamic effect safely. Due to the inertial force effect, the inner radius of the ceramics sleeve may expand only Δb=2.94x10^{-5} mm. Then the shrink fitting ratio may be reduced by only 0.12%. Since the inertial force can be neglected, a quasi-static analysis will be proposed in the following section.

2.3 Coming out simulation for the rotating roller

In this study, the coming out of the shaft will be realized on the numerical simulation. Here, the coming out of the shaft is considered under room temperature because the coming out occurs more easily. When we consider the roller in the heating furnace, equivalent shrink fitting ratios may be applied by considering the shaft expansion because the thermal expansion coefficient of the steel shaft is four times larger than the one of ceramics (see Table 1). Here, the shrink fitting ratio is considered in the range δ/d=0.01x10^{-3}-1.0x10^{-3} at room temperature.

Figure 5 shows the roller rotation under loading where Point A located at the bottom of the shaft moves to the top after rotating 180^o as shown in Figure 5(b). To simulate the coming out behavior, the roll rotation is replaced by the shifted load *w* in the circumferential direction on the fixed roll as shown in Figure 6. The roller is subjected to distributed load *w*=30N/mm as the weight of the conveyed steel assuming the shaft ends are simply supported. As shown in Fig.6, the continuous load shifting can be replaced by discrete load shifting with load shift angle θ_0, which is usually used as a standard discretization numerical analysis. The suitable shift angle will be considered with the numerical results in section 3.3. In other words, the rotation of the roller under loading is replaced by the non-rotating roller subjected to load shifting in the circumferential direction. Then, to obtain the solution numerically, the continuous load shifting is replaced by discrete load shifting in the circumferential direction at the interval θ_0. Here, the initial load position θ_0=0^o is corresponding to the number of cycle N=0, and θ=360^o is corresponding to the number of cycle N=1.

Figure 7 shows the load conditions. Here, a sliding bearing is assumed for the model, which does not constrain the shaft movement. Due to the symmetry Figure 7 show the half model considered with the total number of element 154 320.The smallest element size at the contact portion between sleeve and shaft is 1.25mm x 1.25mm x 6mm. Static structural analysis is performed to the roller by using MSC Marc Mentat 2011 [19] with full Newton-Raphson iterative sparse solver of multifrontal method. In this study, a three-dimensional elastic FEM analysis can be applied because the loading condition does not exceed the yielding stress for the steel shaft, and the macroscopic plastic deformation does not appear for ceramics sleeve until failure.

The effect of the torsional load at the contact portion can be ignored because the shear stress $\tau_{r\theta}$ is very small compared to the shear stress τ_{rz} [13]. In contact analysis, it is known that two types of friction models, that is, stick-slip model and bilinear model have good accuracy [19]. However, since the stick-slip model

needs large amount of data to determine friction force during repetitive calculation process, in this study the bilinear model is applied where the friction force is simply determined from the displacement. The friction coefficient between sleeve and shaft at joint portion is assumed as μ=0.3. All conditions above are used as a reference condition.

3 Evaluation for the coming out and deformation of the shaft due to the distributed load and shrink fitting

3.1 Deformation and stresses of the shaft caused by shrink fitting

In order to consider coming out behavior, the shaft deformation due to shrink fitting is investigated in the first place. Figure 8 illustrates the shaft deformation with the (r,z) coordinate defined before shrink fitting. The displacement u_{zC} in the z-direction is determined from the values at 4 points as $u_{zC}^{sh}=(u_{zA}^{sh}+u_{zA'}^{sh}+u_{zB}^{sh}+u_{zB'}^{sh})/4=u_{zA}^{sh}$ <0 as shown in Figure 8(a). Then, since the shaft is under compression in the r-direction; we have $u_{zA}^{sh}=u_{zC}^{sh}$ <0.

Figure 8(b) shows stress σ_r distribution appearing along the contact surface due to shrink fitting with the maximum compressive stress σ_r=120MPa. Figure 8(c) shows shear stress τ_{rz} distribution due to shrink fitting with the maximum stress τ_{rz} = 30MPa. The shaft is extended in the z-direction by the compressive stress σ_r due to shrink fitting, but the shear stress τ_{rz} may prevent the elongation. Since the shaft end surface tends to be significantly deformed by the compressive stress, the maximum shear stress may be important.

3.2 Displacement and deformation of the shaft due to the initial load

Figure 9(a) shows the shaft after several number of loading cycle N, which defines the displacement u_{zA} at point A and u_{zC} at point C in the (r,z) coordinate. Figure 9(b) shows the shaft due to initial distributed load N=0 focusing on the displacement $u_{zA}^{N=0}$. As shown in Figure 9(b), the positive displacement $u_{zA}^{N=0}$(>0>u_{zA}^{sh}) appears at point A although the displacement due to shrink fitting was negativeu_{zA}^{sh} <0 as shown in Figure 8(a). On the other hand, at point C, the displacement $u_{zC}^{N=0}$(> u_{zC}^{sh}) appears but usually still negative $u_{zC}^{N=0}$<0. Those values $u_{zA}^{N=0}$ and $u_{zC}^{N=0}$ are defined as the initial displacement at N=0 considering both shrink fitting and initial loading.

Figure 10 and Figure 11 show the results of u_{zA} for extremely small δ/d =0.01×10^{-3} and for standard δ/d =0.2×10^{-3}. Here, the friction coefficient μ=0.3 during N=0 to N=3 and the load shift angle θ_0=30° is applied. In Figure 10, Point a' refers to the displacement of shaft due to shrink fitting, while point a represents the initial displacement of the shaft at N=0. Under the small shrink fitting ratio in Figure 10, the average value of the u_{zA} at each cycle increases with increasing N. Under the standard shrink fitting ratio in Figure 11, the average value of the u_{zA} at each cycle is almost constant although the amplitude of u_{zA} increases slightly with increasing N.

Next, the positions of peak and valley of u_{zA} are considered. Figure 10 shows the angle of rotation at point (a), (b), (c), and (d). It is seen that the peak occurs at each number of cycle $N\cong$n+1/6 (n=0,1,2,..) corresponding to the rotation angle $\theta\cong 2\pi n+\pi/3$, while the valley occurs at each number of cycle $N\cong$n+2/3 (n=0,1,2,..) corresponding to the rotation angle $\theta\cong 2\pi n+4\pi/3$. In other words, the peak and valley do not occur

at θ=0° and θ=180°. This is because the relative displacement between the sleeve and shaft cannot follow the load direction change immediately due to the irreversible effect of friction force.

Figure 10 shows displacement u_{zA} of the shaft under low shrink fitting ratio δ/d =0.01×10^{-3}. It is seen that the average displacement u_{zA} increases in the z-direction with increasing the cycle N, that is, the shaft moves in the coming out direction. Under large shrink fitting ratio δ/d =0.2×10^{-3} in Figure 11, although the amplitude of displacement u_{zA} slightly increases with increasing N, the coming out is not seen.

Next, the displacement at point C is considered since at the central point C the cyclic change does not appear. Figure 12 shows the displacement u_{zC} at point C, which increases slightly at the beginning and increases significantly later under δ/d =0.01×10^{-3}. On the other hand, the displacement u_{zC} increases slightly at first and becomes constant under δ/d =0.2×10^{-3}. The possibility of the coming out of the shaft looks small in this case.

3.3 Load shifting angle θ_0 selection

In this study, the roller rotation under bending load is replaced by the non-rotating roller subjected to the load shifting in the circumferential direction. As a standard method of discretization in numerical analysis, the continuous load shifting can be expressed by discrete loads at a certain interval θ_0. Here, a smaller angle θ_0 provides accurate results but large computational time. Therefore, the optimal angle θ_0 should be discussed by investigating u_{zC} with varying the shift angle, θ_0=30°, θ_0=18°, θ_0=12°, and θ_0=6°.

Figure 13 shows u_{zA} under δ/d=0.2x10^{-3} with varying θ_0. Figure 13 shows that smaller θ_0 provides the results for smaller amplitude of u_{zA}. However, the results converge if the $\theta_0 \leq 12°$. The discrete load shift angle θ_0=12° provides 30 data in one cycle, which is enough number to present continuous displacement as shown in Figure 13. Figure 14 shows u_{zC} focusing on the coming out behavior. Although the result for θ_0=30° is very different from others, the results for θ_0=6° and θ_0=12° almost coincide with each other. Since the effect of discrete load shifting is less than 1% if $\theta_0 \leq 12°$, it may be concluded that the load shifting angle θ_0=12° is the most suitable to reduce large calculation time without losing accuracy. In the following calculation the load shift angle θ_0=12° will be used consistently.

4 Effect of mechanical properties on the coming out

In this chapter, effects of several fundamental parameters, such as the shrink fitting ratio, magnitude of the load, Young's modulus, and friction coefficient are considered for the standard model whose geometry of the roller is fixed. Here, the standard model has the following:

the shrink fitting ratio δ/d= 0.4×10^{-3},

the contact length L=300mm,

the friction coefficient between sleeve and shaft μ = 0.3,

the sleeve thicknesses T=30mm,

the shaft thickness t=20mm,

the distributed load on the roller surface is about w=30N/mm,

Young's modulus of the ceramics sleeve E_{sl} =300GPa,

Young's modulus of steel shaft E_{sh} =210GPa.

4.1 Effect of shrink fitting ratio

In this paper, the shrink fitting ratios are considered in the range $\delta/d=0.01\times10^{-3}$-$1.0\times10^{-3}$. Here, $\delta/d=0.01\times10^{-3}$ is an example of low shrink fitting ratio. Next, $\delta/d=0.1\times10^{-3}$, 0.2×10^{-3} , 0.4×10^{-3} may be used for real ceramics roller. Finally, $\delta/d=1.0\times10^{-3}$ is an example of a larger shrink fitting ratio used for steel rollers.

Figure 15(a) shows the results for u_{zC}. With increasing the shrink fitting ratio, the compressive stress increases causing the negative initial value of u_{zC} as shown in Figure 15(a) at N=0. Under low shrink fitting ratio, the displacement u_{zC} increases significantly with increasing N. The coming out speed is shown in Figure 15(b). To clarify the coming out behavior, the speed of the coming out is defined as $(u_{zC}|_N-u_{zC}|_{N-0.5})/0.5$. Under $\delta/d=0.01\times10^{-3}$-$0.1\times10^{-3}$, the speed increases with increasing N at N=0-5. Under $\delta/d=0.2\times10^{-3}$ the coming out speed is small, then increases after N=4. Under $\delta/d=0.4\times10^{-3}$ although the speed increases slightly at the beginning, but after N=3 the speed becomes almost zero. Under $\delta/d=1.0\times10^{-3}$ the displacement u_{zC} is always negative and the speed is always zero independent of N. In the following analysis $\delta/d=0.4\times10^{-3}$ is considered as a reference condition.

4.2 Effect of the magnitude of the load

The distributed load w=30N/mm is applied to the sleeve from conveyed steel as shown in Figure 7. In Figure 16 the effects of the magnitude of load is investigated for w=15, 45, 60N/mm. The coming out speed significantly increases with increasing the magnitude of the load. It is seen that the coming out accelerates at N=0-4. In other words, the coming out easily occurs when the distributed load $w\geq$45N/mm.

4.3 Effect of Young's modulus of the Shaft

Figure 17 shows the effect of Young's modulus of the shaft. Three types of Young's modulus are considered, namely E_{sh} = 210GPa corresponding to steel, E_{sh} = 300GPa corresponding to the silicon nitride ceramics, and E_{sh} = 100GPa corresponding to flake graphite cast iron. The smaller Young's modulus causes larger displacement u_{zC} as well as the larger initial value in the negative at N=0 as shown in Figure 17 because of the larger deformation of the shaft. It is seen that when Young's modulus of shaft $E_{sh}\leq$100GPa the u_{zC} increases significantly with increasing number of cycle N.

4.4 Effect of the friction coefficient

Figure 18 (a) shows the effect of the coefficient of friction between the ceramics sleeve and steel shaft. The displacement u_{zC} increases with increasing N especially under smaller value of μ. However, when μ=0.1, the behavior of u_{zc} is quite different from others because the u_{zc} has a peak at N=1.5 and increases again at N=2.5 and finally increases rapidly after N=3. Figure 18(b) shows the coming out speed clearly although most of the speed is nearly zero except for the result of μ=0.1 after N=3. Figure 18 indicates that when $\mu\leq$0.1 the coming out happens very easily.

5 Effect of shaft geometry on the coming out

5.1 Effect of the shaft thickness

In the real ceramic rollers, the shaft should be designed so as to prevent the coming out. The effect of shaft geometry is considered in this chapter. Similar to the previous discussion of the shaft Young modulus, the rigidity of the shaft can be also considered by varying the shaft thickness t. Figure 19(a),(b) show the results for different shaft thickness t=10mm, t=20mm, t=40mm under $\delta/d = 0.4\times10^{-3}$. It is seen that u_{zC} becomes larger for smaller thickness t. The difference between the results for t=10mm and t=20mm is much larger than the one for t=20mm and 40mm. For t=10mm, the coming out speed tends to increase during N=0-4 but becomes stable at about 0.02mm/cycle after N=4. Therefore Figure 19(b) suggests that steady coming out may appear if the number of cycle N is large enough. Since the coming out speeds for t=20 and t=40mm are very small, the rigidity may be enough to prevent the coming out. From Figure 19(a) and 19(b), it may be concluded that when $t \leq 10$mm the coming out occurs.

5.2 Effect of the contact length of the shaft

The standard model has contact length L=300mm. To investigate the effect of L on u_{zC}, Figure 20(a) shows the results for L=120mm, L=150mm, L=240mm, L=480mm. Figure 20(a) shows when L is smaller, the displacement u_{zC} becomes larger. This is due to the larger contact length L having larger friction force.

Figure 20(b) shows the speed of the coming out. To clarify the coming out behavior, the speed of the coming out of the shaft is defined as $(u_{zC}|_N - u_{zC}|_{N-0.5})/0.5$. The speed of the coming out becomes steady if N is large enough except for L=150. For L=450mm, the speed is zero from N=0. And for L=300mm, the steady speed appears after N=3. The results for L=480mm and L=300mm indicate that the coming out is hard to occur. On the other hand, the speed increases with increasing number of cycle for L=225mm and L=150mm after N=4, which means the coming out occurs easily.

6 The coming out mechanism

The coming out of the shaft has been realized in the numerical simulation as shown in previous chapters. The results are different depending on the shrink fitting ratio and other parameters. Since it is difficult to obtain the results for large number N because of large calculation time, it is desirable that we can judge the coming out appears or not even when N is small. In this chapter, the coming out mechanism is considered by focusing on the stress distribution appearing at the contact portion.

6.1 Investigation of shear stress τ_{rz} at contact portion due to small friction coefficient

Effects of the mechanical properties and shaft geometry on the coming out have been investigated in chapter 4 and 5. However, the unique result appears for small friction coefficient effect as shown in Figure 18. Here, the result for μ=0.1 shows that the behavior of u_{zc} is quite different from others. This phenomenon is interesting to be investigated.

To understand the result for μ=0.1in Figure 18, shear stress τ_{rz} is investigated along the contact surface. Figure 21 shows the shear stress distribution at the lower portion $\tau_{rz}(z)|_{\theta=180^\circ}$ for different N. Note that the value of $\tau_{rz}(0)|_{\theta=180^\circ}$ increases with decreasing the FEM mesh size, but if $z \geq 4$mm the value of $\tau_{rz}(z)|_{\theta=180^\circ}$ becomes mesh-independent. Figure 22 shows the value of $\tau_{rz}(z=5\text{mm})|_{\theta=180o}$ for friction coefficient μ=0.1, 0.3,

0.5. Differently from the results for μ=0.3, 0.5, the shear stress for μ=0.1 becomes zero after N=3. It should be noted that the average value of shear stress $\tau_{rz}(z)|_{\theta=180^\circ}$ is nearly zero after N=3. Since the average value is nearly zero, the coming out of the shaft occurs easily without resisting the friction force due to small μ.

6.2 The coming out judgement based on shear stress distribution along contact surface

Figure 23 shows shear the stress distribution τ_{rz} along the shaft half surface for $\theta=0^o$~180^o when N=3. Figure 23(a) shows the shear stress distribution under low shrink fitting ratio $\delta/d=0.01\times10^{-3}$ where the coming out is likely to occur, and Figure 23(b) shows the result under large shrink fitting ratio $\delta/d=1.0\times10^{-3}$ used for steel components. Figure 23 shows the stress distributions are very different each other. For example, in Figure 23(a), the stress τ_{rz} changes in the circumferential direction quite largely. On the other hand in Figure 23(b), the stress τ_{rz} does not change in the circumferential direction. The stress variation in Figure 23(a) is due to the effect of the bending load. Figure 23(b) is depending on the large shrink fitting stress with small effect of bending load.

Figure 24(a) focuses on the stresses along the lines $\theta=0^o$ and 180^o. Here, $\tau_{rz}\big|_{\theta=0^\circ}$ and $\tau_{rz}\big|_{\theta=180^\circ}$ are compared between N=0 and 3 under $\delta/d=0.01\times10^{-3}$. The shear stress due to shrink fitting is approximately equal to zero except at both ends when N=0.Therefore, when N=3, the shear stress at shrink fitting is greatly changed, and the shear stress directions are reversed at both shaft ends. The shear stress at the left end tries to prevent the coming out of the shaft.

In Figure 24(b), $\tau_{rz}\big|_{\theta=0^\circ}$ and $\tau_{rz}\big|_{\theta=180^\circ}$ are compared between N=0 and N=3 under $\delta/d=1.0\times10^{-3}$. When N=0, it is seen the maximum value $\tau_{rz}\big|_{max}$=30 MPa is about 600 times larger than the maximum value $\tau_{rz}\big|_{max}$=0.05 MPa in Figure 24(a). Although not indicated, the maximum compressive stress in Figure 24(b) is about 180 times larger than the maximum compressive stress in Figure 24(a). Due to those large shrink fitted stresses, as shown in Figure 24(b), the effect of the bending load becomes smaller and stress does not change very much between N=0 and N=3 under $\delta/d=1.0\times10^{-3}$.

7 Conclusions

This paper dealt with failure analysis for coming out of the steel shaft from ceramics sleeve connected by shrink fitting. Here, inner diameter of the sleeve d=240mm is considered. Only low shrink fitting ratio can be applied because of the brittleness of the ceramics sleeve. In this study, the coming out behavior of the roller during rotation was analyzed by the finite element method. The conclusions can be summarized as follows:

1. In the numerical analysis the rotation of the roller under loading is replaced by the non-rotating roller subjected to shifting load in the circumferential direction. As a standard method of discretization in numerical analysis, the continuous load shifting can be replaced by discrete load shifting with less than 1% error if the load shifting interval angle $\theta_0\leq12^o$.
2. It is confirmed that the inertial force can be neglected and the quasi-static analysis presented in this paper is accurate enough.

3. The coming out of the shaft can be realized by numerical simulation. The coming out of the shaft appears under smaller shrink fitting ratio $\delta/d \leq 0.2 \times 10^{-3}$ and does not appear under larger shrink fitting ratio $\delta/d \geq 0.4 \times 10^{-3}$ as shown in Figure 15.
4. The coming out happens easily for smaller Young's modulus of the shaft $E_{sh} \leq 100$GPa, smaller friction coefficient $\mu \leq 0.1$, and larger distributed load $w \geq 45$N/mm.
5. The speed of coming out can be prevented by increasing thickness of the shaft $t \geq 20$mm in Figure 21 and contact length $L \geq 300$mm as shown in Figure 22.
6. The shear contact stress is changed largely between N=0 and N=3 if the coming out happens, and does not change very much if no coming out. The shear contact stress change may be useful information to judge the coming out appears or not.

References

[1] Fujii M, Yoshida A, Ishimaru J, Shigemura S, and Tani K. Influence of sprayed layer thickness on rolling contact fatigue of ceramics sprayed roller, *Transactions of the JSME Series C* 2006; 72(716): 1354-1360. (in Japanese)

[2] Ono T. Current status and future prospect of the development of high performance ceramics, *Journal of the Japan Society of Mechanical Engineers* 1983; 86(774): 470-475. (in Japanese)

[3] Liou CR, Mori T, Kobayashi H, Mitamura T. Influence of Various Atmosphere on the Corrosion resistance of Si3N4 sintered bodies against steel making slag and its main components, Journal of Ceramic Society of Japan 1990; 98(4): 348-354.

[4] Noda NA Hendra, Takase Y, and Tsuyunaru M. Maximum stress for shrink fitting system used for ceramics conveying rollers, *Journal of Solid Mechanics and Materials Engineering* 2008; 2(8): 1410-1419.

[5] Li W, Noda NA, Sakai H, and Takase Y. Analysis of Separation Conditions for Shrink Fitting System Used for Ceramics Conveying Rollers, *Journal of Solid Mechanics and Materials Engineering* 2011; 5(1): 14-24.

[6] Li W, Noda NA, Sakai H, and Takase Y. Thermal Stress Analysis for Shrink fitting System used for Ceramics Conveying Rollers in the Process of Separation, *Key Engineering Materials* 2011; 452-453: 241-244.

[7] Dedi S, Noda NA, Sano Y and Takase Y. Ceramics/steel joint selection for the ceramics roller used at high temperature, *Proceeding of the 4th ACEE 2014*; 221-222

[8] Harada S, Noda NA, Uehara O, and Nagano M. Tensile strength of hot isostatic pressed silicon nitride and effect of specimen dimension, *Transactions of the JSME Series A* 1991; 57(539): 1637-1642. (in Japanese)

[9] Ogawa E, Shimizu K, and Hamayoshi S. Practical evaluation of large ceramic rolls for continuous hot dipping steel sheet production line, *Hitachi Metals Technical Review* 2012: 28: 50-55. (in Japanese)

[10] Noda NA, Yamada M, Sano Y, Sugiyama S, and Kobayashi S. Thermal Stress for All-Ceramics Rolls Used in Molten to Produce Stable High Quality Galvanized Steel Sheets, *Engineering Failure Analysis* 2008; 15(4): 261-274.

[11] Ogawa E, et. al. Development of 100% ceramic pot rolls for continuous hot dip coating lines of the steel sheet, *Proceedings of 8th International Conference on Zinc and Zinc Alloy Coated Steel Sheet* 2011; 6: 1-8.

[12] Noda NA, Hendra, Oosato M, Suzumoto K, Takase Y, and Li W. Strength Analysis for Shrink Fitting System Used for Ceramics Rolls in the Continuous Pickling Line, *Key Engineering Materials* 2011; 462-463: 1140-1145.

[13] Matsuda S, Suryadi D, Noda NA, Sano Y, Takase Y, and Harada S. Structural Design for Ceramics Rollers Used in the Heating Furnace, *Transactions of the JSME Series A* 2013; 79(803): 989-999. (in Japanese)

[14] Truman CE, Booker JD. Analysis of a Shrink-fit Failure on a Gear Hub/Shaft Assembly, *Engineering Failure Analysis* 2007; 14: 557-572.

[15] Antoni N, Contact Separation and Failure Analysis of a Rotating Thermo-elastoplastic Shrink-fit Assembly, *Applied Mathematical Modelling* 2003; 37: 2352-2363.

[16] Rusin A, Nowak G, Piecha W. Shrink connection modelling of the steam turbine rotor, Engineering Failure Analysis 2013; 34: 217-227.

[17] Iron and Steel Institute of Japan. Steel Handbook. pp. 886-887, Tokyo: Maruzen co., Ltd.: 1962

[18] Timoshenko SP and Goodier JN. Theory of Elasticity. pp. 81-82, Tokyo: McGraw-Hill Kogakusha Ltd.: 1970

[19] Marc Mentat team. Theory and User Information. Vol. A. pp.532, Tokyo: MSC. Software: 2008.

Figure Captions

Figure 1 Layout of rollers in heating furnace

Figure 2 Roller structure (a) Conventional roller; (b) New roller

Figure 3 Structure and dimensions of the new roller model with standard dimensions (mm).

Figure 4 Two-dimensional of rotating disk with a circular hole.

Figure 5 Dimensions and loading condition of new roller (a) Initial state; (b) 180°rotation

Figure 6 The rotation of the roller replaced by the shifted load at the interval of the load shift angle θ_0. When θ=0°the number of cycle N=0, and when θ=360°the number of cycle N=1.

Figure 7 Standard half model with FEM mesh.

Figure 8 The z-displacement and stress of the shaft due to shrink fitting (a) The z-displacement due to shrink fitting $u_{zC}^{sh} = (u_{zA}^{sh} + u_{zA'}^{sh} + u_{zB}^{sh} + u_{zB'}^{sh})/4 = u_{zA}^{sh} < 0$; (b) Stress σ_r due to shrink fitting; (c) Stress τ_{rz} due to shrink fitting

Figure 9 The z-displacement of the shaft due to bending load. (a) Definition of z-displacement u_{zA}, u_{zC} after several number of cycle N; (b) The z-displacement due to shrink fitting and initial load

Figure 10 The z-displacement at point A u_{zA} vs. number of cycle N for δ/d=0.01×10^{-3} and μ=0.3 when θ_0= 30°.

Figure 11 The z-displacement at point A u_{zA} vs. number of cycle N for δ/d=0.2×10^{-3} and μ=0.3when θ_0=30°.

Figure 12 The displacement point C u_{zC} vs. number of cycle N for different shrink fitting ratio when θ_0=30°.

Figure 13 The z-displacement at point A u_{zA} vs. number of cycle N for different θ_0 at δ/d =0.2×10^{-3} and μ=0.3

Figure 14 The z-displacement at center point C u_{zC} vs. number of cycle N for different θ_0 when δ/d =0.2×10^{-3} and μ=0.3

Figure 15 Effect of the shrink fitting ratio on the coming out of the shaft (a) u_{zC} vs. Number of cycle N; (b) speed of the coming out

Figure 16 Effect of distributed load when δ/d=0.4x10^{-3}

Figure 17 Effect of Young's modulus of the shaft when δ/d=0.4x10^{-3}

Figure 18 Effect of the friction coefficient when δ/d=0.4x10^{-3} (a) u_{zC} vs. Number of cycle N; (b) speed of the coming out

Figure 19 Effect of the contacted shaft thickness when δ/d=0.4x10^{-3} and μ=0.3 (a) u_{zC} vs. Number of cycle N; (b) speed of the coming out

Figure 20 Effect of the contact length when δ/d=0.4x10^{-3} and μ=0.3 (a) u_{zC} vs. Number of cycle N; (b) speed of the coming out

Figure 21 Shear stress distribution along contact potion with variation of the number of cycle N when δ/d=0.4x10^{-3}

Figure 22 Shear stress τ_{rzA} vs. number of cycle N when δ/d=0.4x10^{-3}

Figure 23 Shear stress distribution τ_{rz} from θ=0° to θ=180° at N=3 for (a) δ/d =0.01×10^{-3} and (b) δ/d =1.0×10^{-3}.

Figure 24 Shear stress distribution τ_{rz} from θ=0° to θ=180° at shrink fitting and N=3 for (a) δ/d =0.01×10^{-3} and (b) δ/d =1.0×10^{-3}.

Table Captions

Table 1 Properties of materials

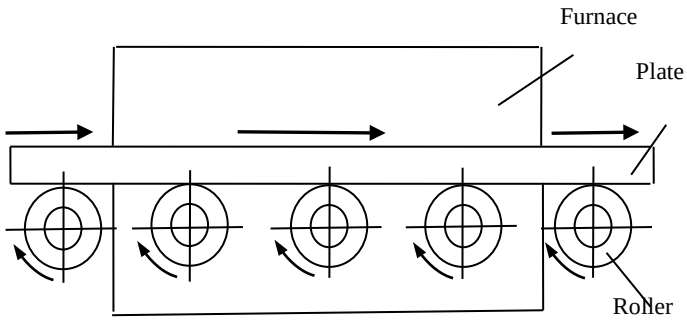

Fig.1 Layout of rollers in heating furnace

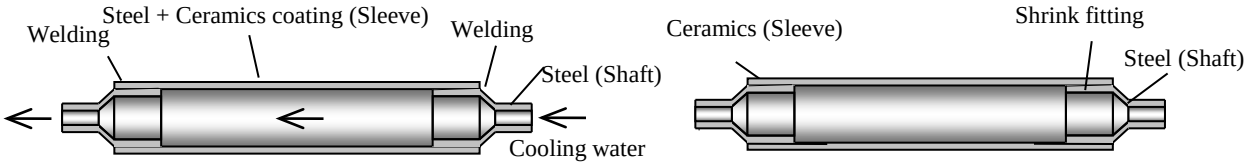

(a) Conventional roller (b) New roller

Fig.2 Roller structure

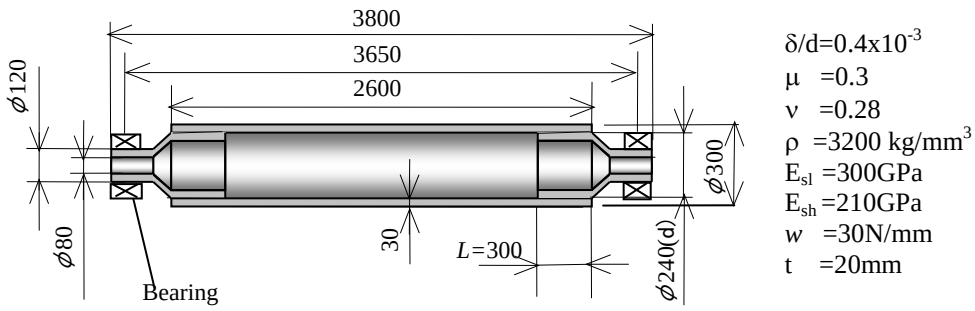

Fig.3 Structure and dimensions of the new roller model with standard dimensions(mm).

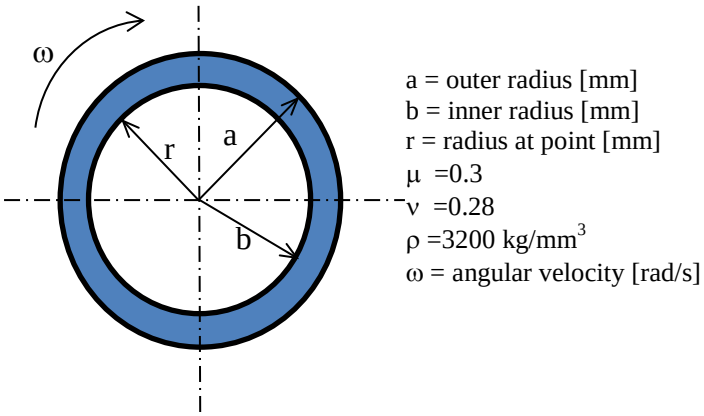

Figure 4 Two-dimensional of rotating disk with a circular hole

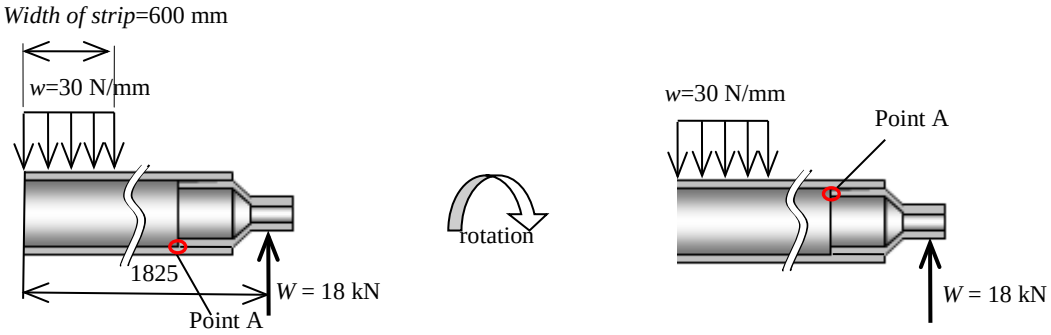

(a) Initial state (b) 180°rotation

Fig.5 Dimensions and loading condition of new roller

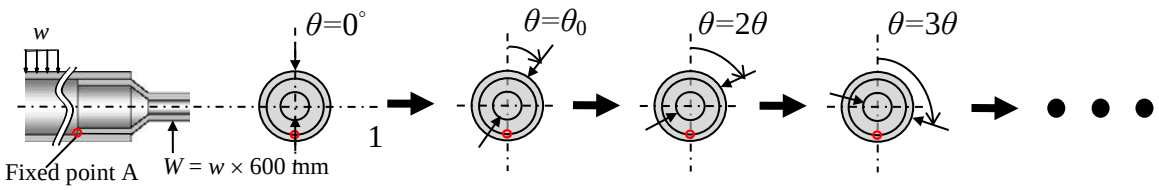

Fig.6 The rotation of the roller replaced by the shifted load at the interval of the load shift angle θ_0. When θ=0°the number of cycle N=0, and when θ=360° the number of cycle N=1.

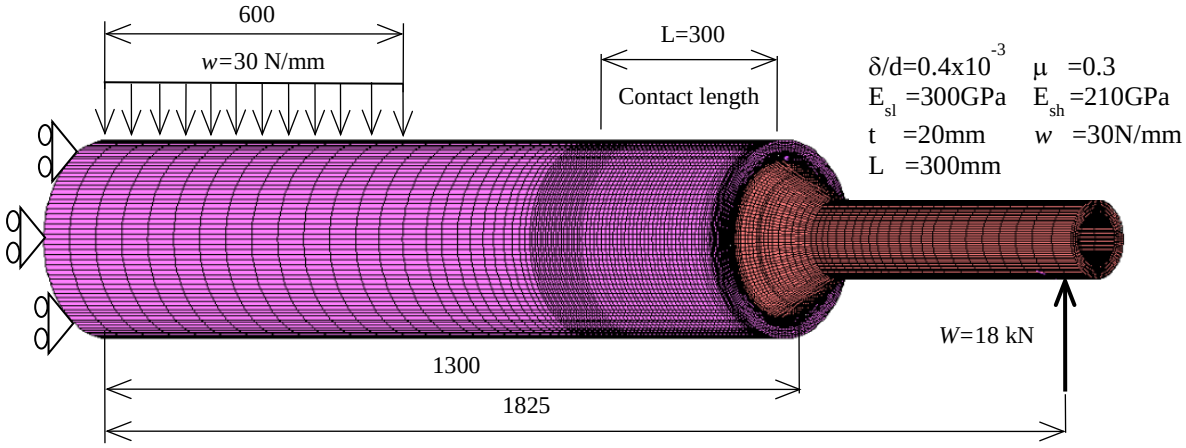

Fig.7 Standard half model with FEM mesh.

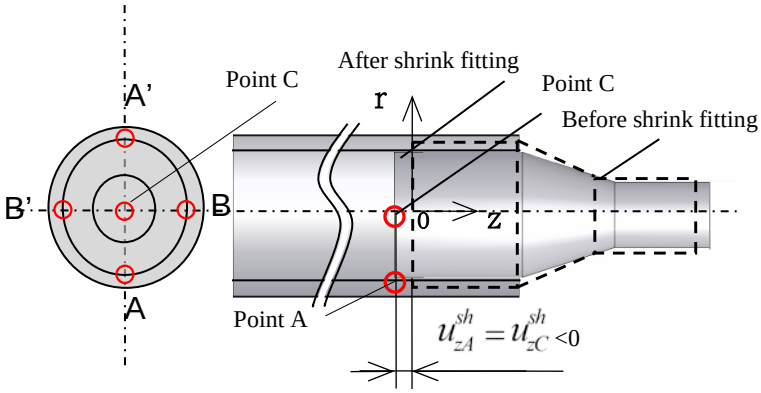

(a) Displacement due to shrink fitting $u_{zC}^{sh} = (u_{zA}^{sh} + u_{zA'}^{sh} + u_{zB}^{sh} + u_{zB'}^{sh})/4$

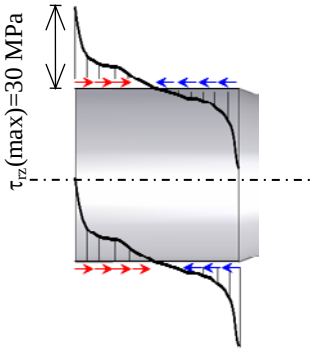

(c) Stress τ_{rz} due to shrink fitting

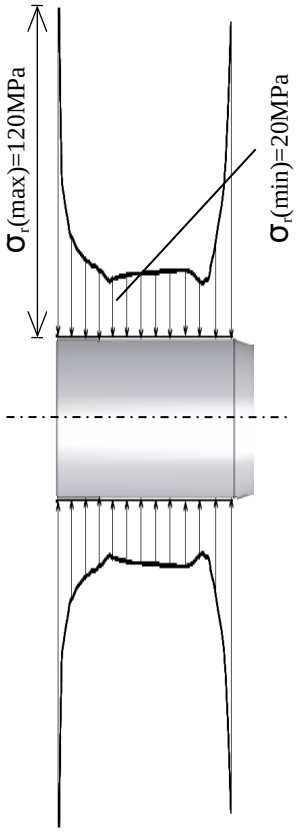

(b) Stress σ_r due to shrink fitting

Fig.8 The z-displacement and stress of the shaft due to shrink fitting

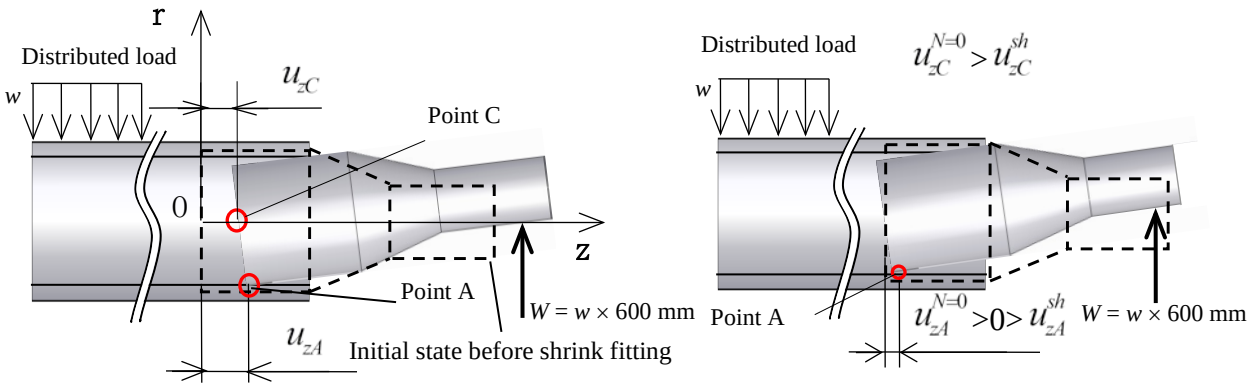

(a) Definition of z-displacement u_{zA}, u_{zC} after several number of cycle N

(b) The z-displacement due to shrink fitting and initial load

Fig.9 The z-displacement of the shaft due to bending

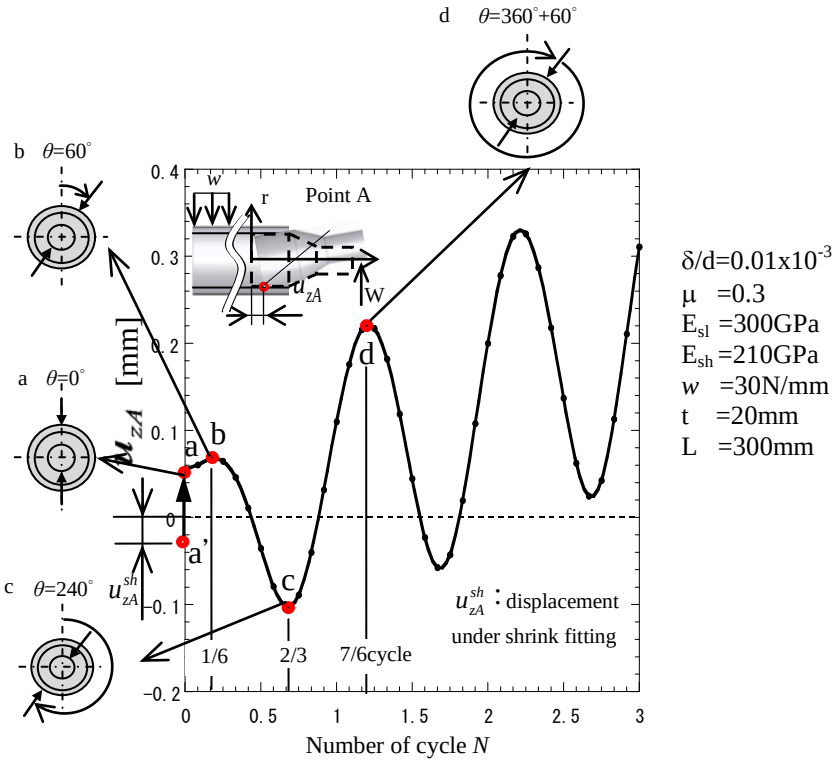

Fig. 10 The z-displacement at point A u_{zA} vs. number of cycle N for δ/d=0.01×10^{-3} and μ=0.3 when θ_O=30°.

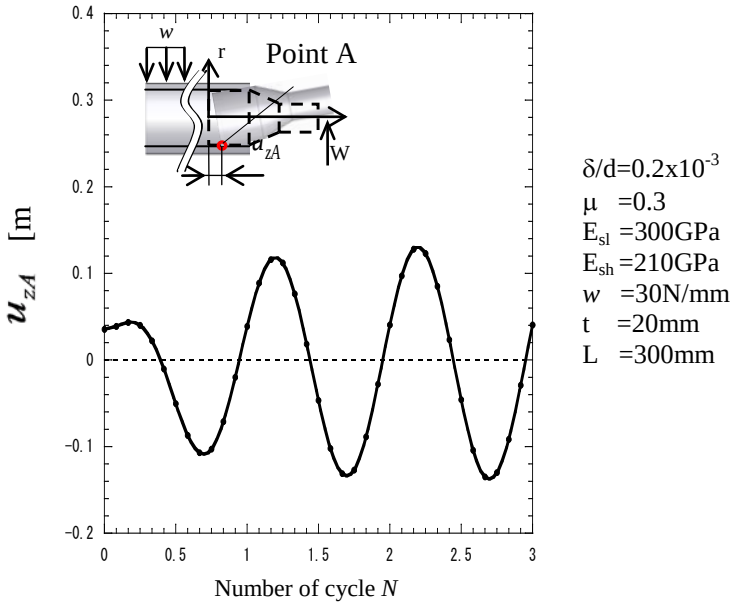

Fig.11 The z-displacement at point A u_{zA} vs. number of cycle N for δ/d=0.2×10^{-3} and μ=0.3when θ_O=30°.

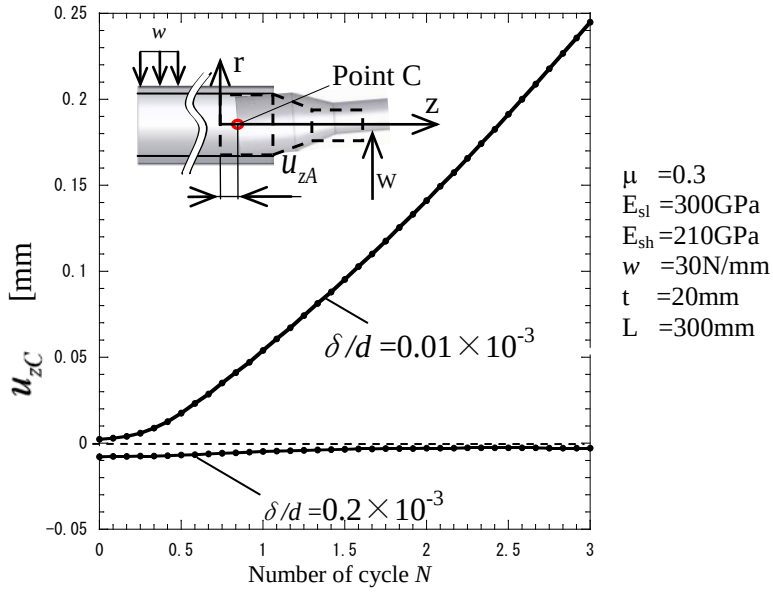

Fig.12 The z-displacement at point C u_{zC} vs. number of cycle N for different shrink fitting ratio when θ_0＝30°.

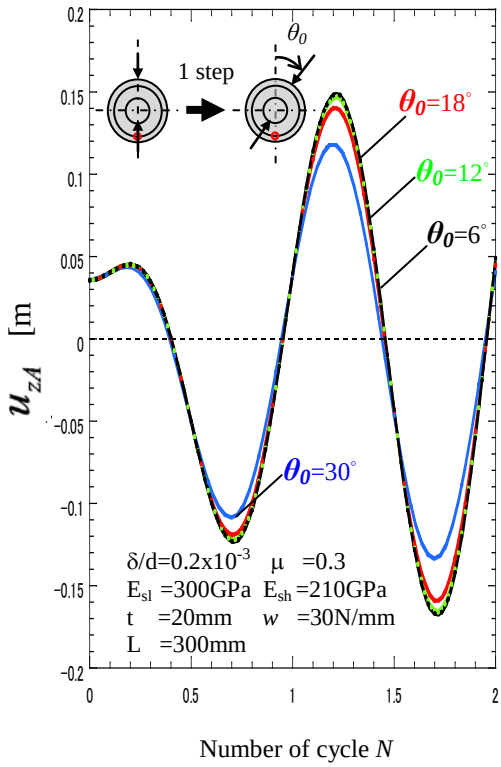

Fig.13 The z-displacement at point A vs. number of cycle N for different θ_0 at $\delta/d = 0.2\times10^{-3}$ and $\mu=0.3$

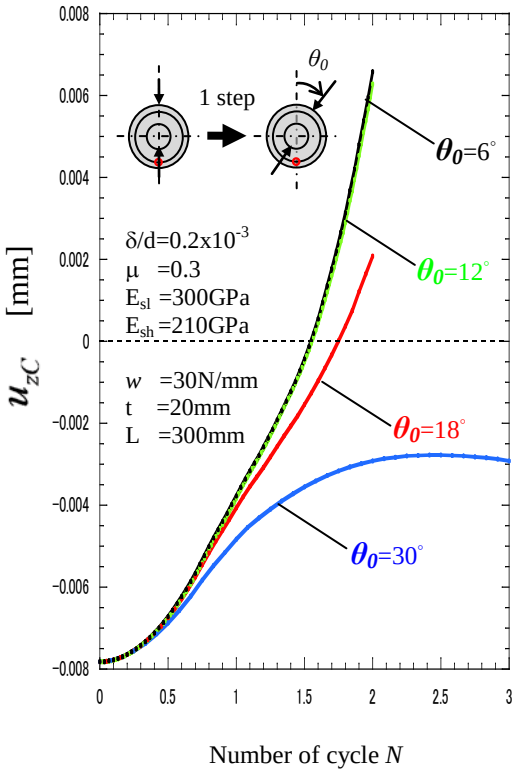

Fig.14 The z-displacement at center point C vs. number of cycle N for different θ_0 when $\delta/d = 0.2\times10^{-3}$ and $\mu=0.3$

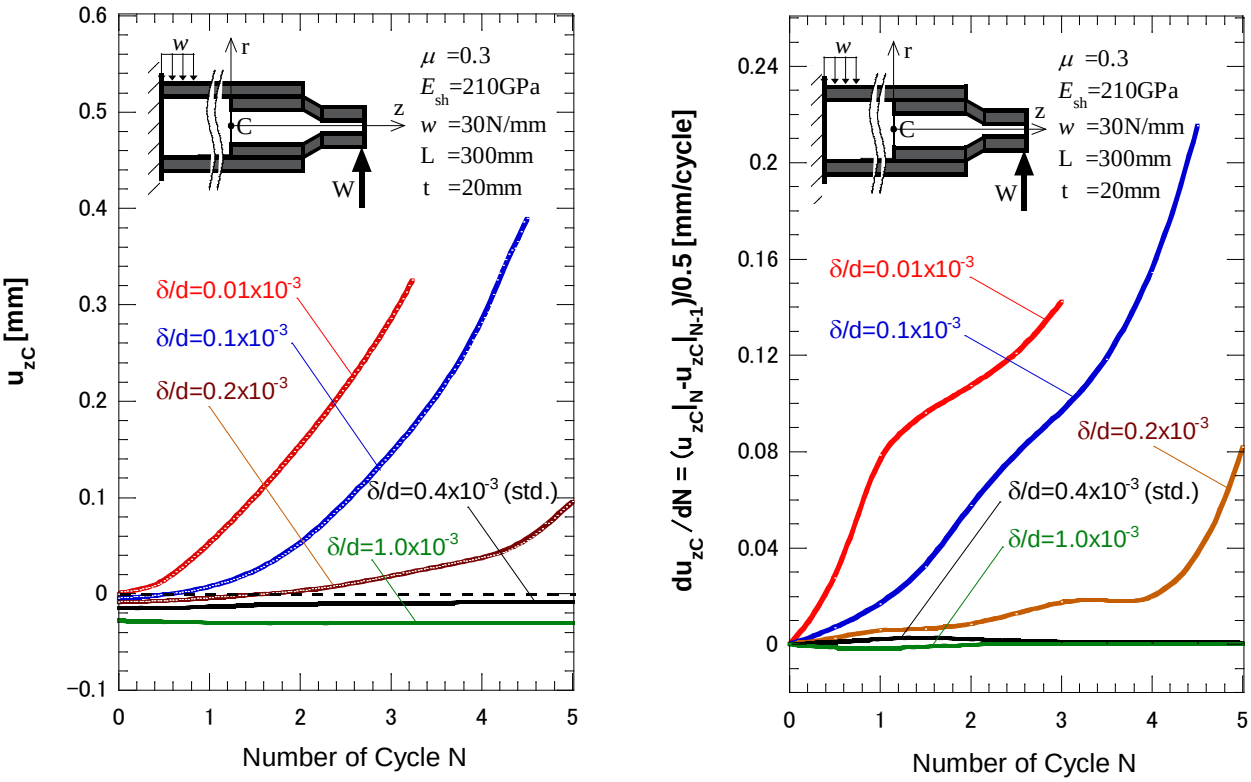

(a) u_{zC} vs. number of cycle N

(b) Speed of the coming out

Fig. 15 Effect of the shrink fitting ratio on the coming out of the shaft

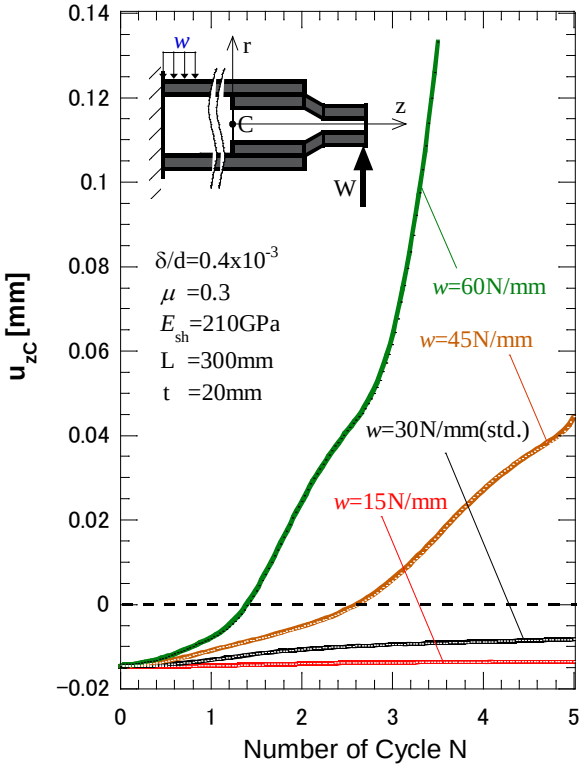

Fig. 16 Effect of distributed load when $\delta/d=0.4\times10^{-3}$

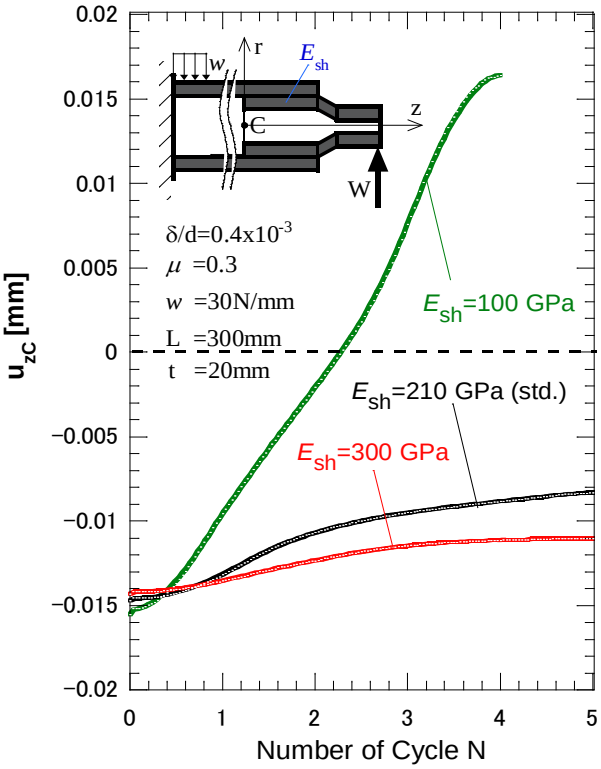

Fig. 17 Effect of Young's modulus of the shaft when δ/d=0.4x10^{-3}

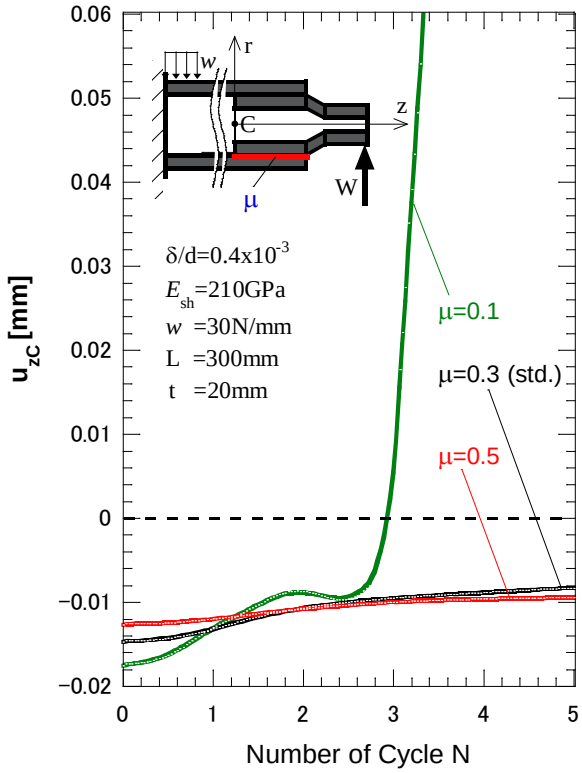

(a) u_{zC} vs. number of cycle N

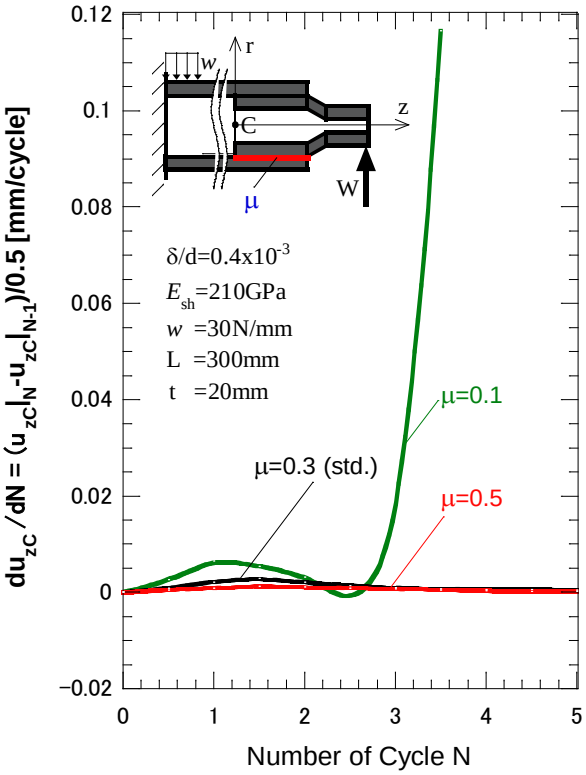

(b) Speed of the coming out

Fig. 18 Effect of the friction coefficient when δ/d=0.4x10^{-3}

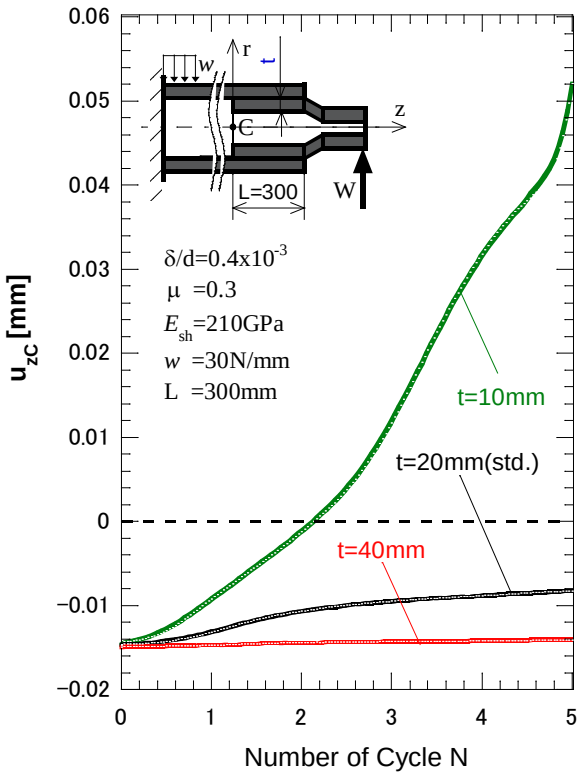

(a) u_{zC} vs. number of cycle N

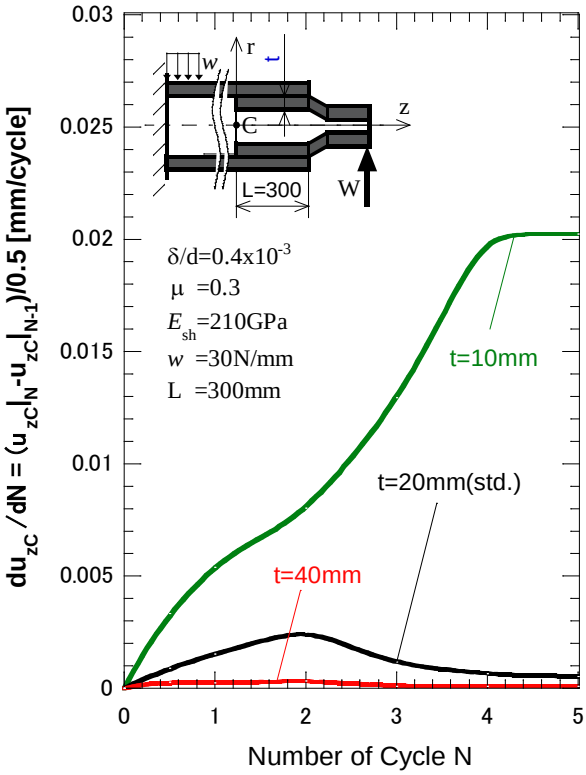

(b) Speed of the coming out

Fig. 19 Effect of the contacted shaft thickness when δ/d=0.4x10^{-3} and μ=0.3

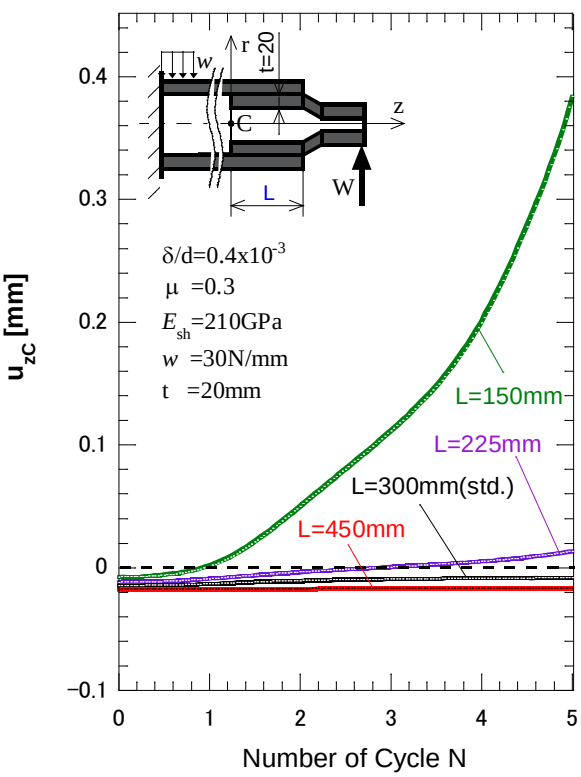

(a) u_{zC} vs. number of cycle N

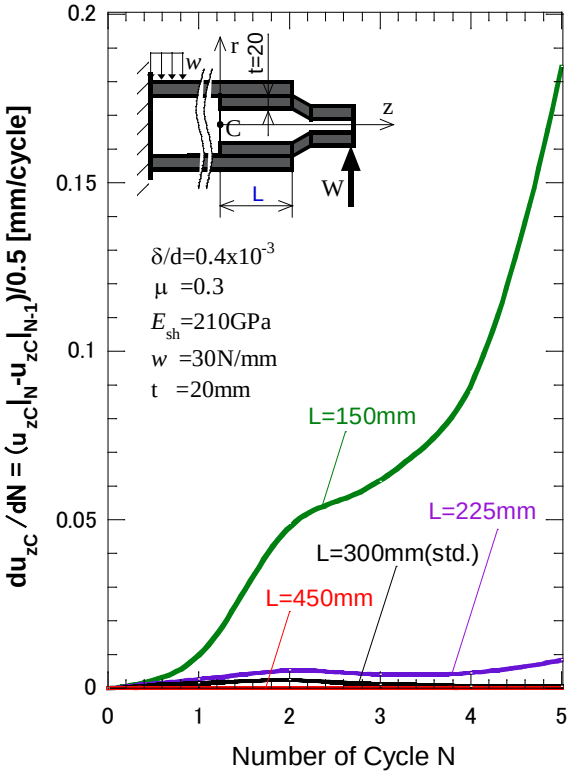

(b) Speed of the coming out

Fig. 20 Effect of the contact length when $\delta/d=0.4\times10^{-3}$ and $\mu=0.3$

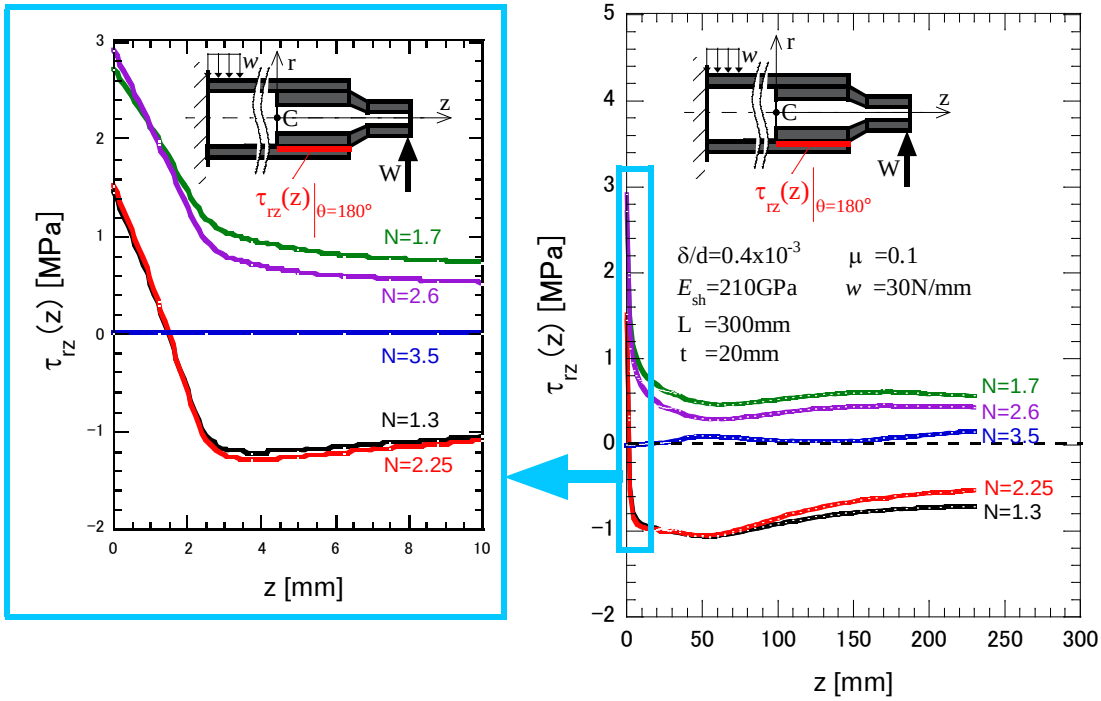

Fig. 21 Shear stress distribution along contact portion with variation of the number of cycle N when$\delta/d=0.4\times10^{-3}$ and $\mu=0.1$

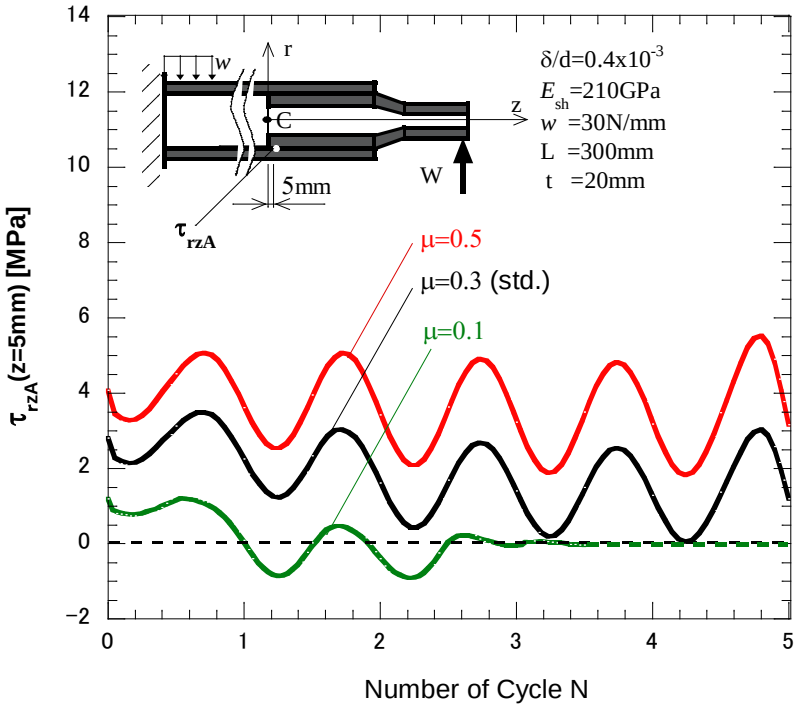

Fig. 22 Shear stress τ_{rzA} vs. number of cycle N when $\delta/d=0.4\times10^{-}$

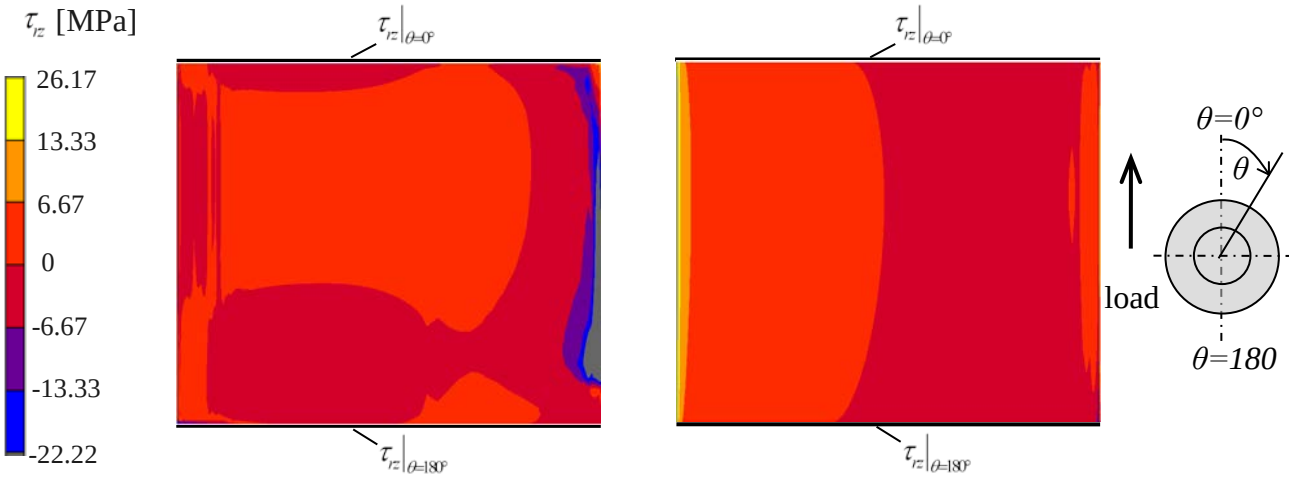

(a) δ/d =0.01×10^{-3} (b) δ/d =1.0×10^{-3}

Fig.23 Shear stress distribution τ_{rz} from θ=0° to θ=180° at N=3 for (a) δ/d =0.01×10^{-3} and (b) δ/d =1.0×10^{-3}.

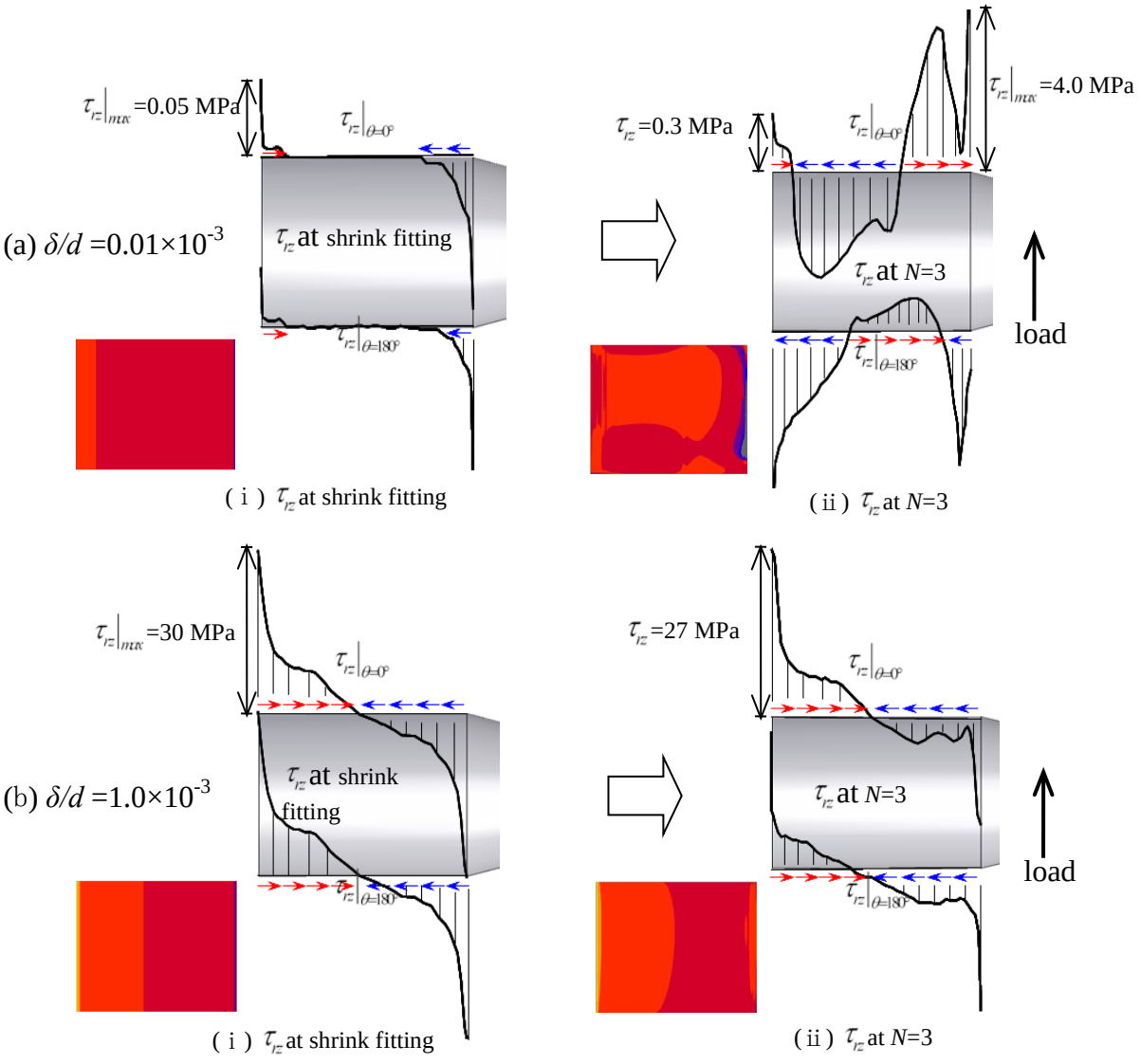

Fig.24 Shear stress distribution τ_{rz} from θ=0° to θ=180° at shrink fitting and N=3 for (a) δ/d =0.01×10^{-3} and (b) δ/d =1.0×10^{-3}.

Table 1 Properties of materials

Properties	**Ceramics**	**Steel**
Young's modulus [GPa]	300	210
Poisson's ratio	0.28	0.3
Tensile strength [MPa]	500	600
Mass density [kg/m^3]	3200	7800
Thermal expansion coefficient [1/K]	$0.3x10^{-5}$	$1.2x10^{-5}$